MITSUBISHI ELECTRIC RESEARCH LABORATORIES
http://www.merl.com

Sparsity-Driven Radar Auto-Focus Imaging Under Over-Wavelength Position Perturbations

Liu, D.

TR2016-083 July 2016

Abstract

We consider a 2D imaging problem where a perturbed mono-static radar is used to detect localized targets situated in a region of interest. In order to deal with position-induced out-of-focus, we proposed a sparsity-driven auto-focus imaging approach in which each radar measurement is modeled as a superposition of weighted and delayed target signatures scattered from the corresponding target phase centers. We iteratively exploit the position-related delays and the target signatures by analyzing data coherence, and consequently form an adaptive projection matrix of the radar measurements. By imposing sparsity on the scattering weights, a sparse image and a dense image, without and with the target signatures respectively, are reconstructed. Compared to existing auto-focus methods, our approach significantly improves radar focus performance in imaging localized targets, even under position perturbations up to 10 wavelengths of the radar central frequency. We validate our algorithm with simulated noisy data.

The Ninth IEEE Sensor Array and Multichannel Signal Processing Workshop

Sparsity-Driven Radar Auto-Focus Imaging Under Over-Wavelength Position Perturbations

Dehong Liu
Mitsubishi Electric Research Laboratories
Cambridge, MA 02139
Email: liudh@merl.com

***Abstract*—We consider a 2D imaging problem where a perturbed mono-static radar is used to detect localized targets situated in a region of interest. In order to deal with position-induced out-of-focus, we proposed a sparsity-driven auto-focus imaging approach in which each radar measurement is modeled as a superposition of weighted and delayed target signatures scattered from the corresponding target phase centers. We iteratively exploit the position-related delays and the target signatures by analyzing data coherence, and consequently form an adaptive projection matrix of the radar measurements. By imposing sparsity on the scattering weights, a sparse image and a dense image, without and with the target signatures respectively, are reconstructed. Compared to existing auto-focus methods, our approach significantly improves radar focus performance in imaging localized targets, even under position perturbations up to 10 wavelengths of the radar central frequency. We validate our algorithm with simulated noisy data.**

***Keywords*—Auto-focus, radar imaging, sparsity, data coherence**

I. Introduction

Radar imaging is an inverse problem to determine the reflectivity of a region of interest (ROI) given the transmitted source signals, the corresponding received echoes, and the transmitting and receiving antenna positions. When the antenna positions are known, a simple delay-and-sum method is able to perform well-focused imaging by compensating the phase changes of the received echoes.

However, in radar applications, it is very common that the exact antenna positions are not available due to environment interference or imprecise motion control of the radar platform. For example, for a vehicle mounted mono-static radar system, as the vehicle is moving along some predesigned trajectory, position perturbations are introduced due to the non-smooth road surface or the varying driving velocity, *etc*. These position perturbations can be as large as several wavelengths of the radar center frequency. Although modern navigation systems such as the Global Positioning System (GPS) can measure positions with a high accuracy, the range of resulting errors is still beyond the requirements of high-resolution radar imaging. In such a situation, if the phase changes are not well compensated in the imaging process, the final radar images will be out of focus.

Auto-focus has been a challenging problem in the radar imaging field as well as other array imaging fields of different sensor modalities. Existing radar auto-focus methods can be roughly grouped into two categories. One is based on phase compensation [1]–[3], and the other is based on position or motion compensation [4]–[6]. The phase-compensation based methods seek to compensate data phases in terms of different merits such as the entropy or the total energy of residuals, to generate an overall well-focused image. These methods generally work well in compensating environment-induced phase distortions, but poorly in compensating antenna position-induced phase errors since the position-induced phase errors are generally different for different imaging positions in the ROI. The position or motion compensation based methods, on the other hand, seek to compensate position errors by analyzing radar movements such that the position-induced phase errors can be well corrected across the whole ROI [4], [5]. These motion-compensation methods are effective for fast-moving radar platforms in deblurring radar images, but not suitable for radars with random position perturbations. In recent years, with the introduction of compressive sensing (CS) to the radar imaging community, auto-focus imaging is formulated as a CS reconstruction problem [6]–[8], where radar signals are modeled as CS measurements of the underlying sparse reflectivity of the ROI via a perturbed projection matrix, and each target in the ROI corresponds to a cluster of non-zero scattering points to be reconstructed. The CS reconstruction errors, although bounded by a factor of the positions errors [9], [10], increase dramatically when the unknown position errors are comparable to the radar central wavelength. A valid CS solution is achievable only when the position errors are much smaller than the wavelength. When the position errors are in the order of several wavelengths, the CS-based methods typically fail to converge to the right solution due to the phase wrapping issue.

In this paper, we propose an auto-focus imaging approach based on data coherence analysis and image sparsity. In the approach, each radar target is characterized by a single phase center and its own scattering signature. Radar measurements are then modeled as weighted sums of delayed target scattering signatures, with weights associated with the corresponding target scattering coefficients and the antenna patterns, and delays related to distances between the target phase centers and the unknown antenna positions. We then iteratively exploit the delays using data coherence analysis and adaptively extract the target signatures to generate the bases of the CS projection matrix. The focused radar image is then reconstructed by imposing sparsity on the weights. The main advantage of our sparsity-driven autofocus approach over the other CS-based autofocus algorithms is that our approach is capable of compensating random position perturbations up to several wavelengths and yielding well-focused images. We verify our approach with a set of simulated noisy data.

II. Data acquisition model

We consider a 2D radar imaging problem in which a mono-static moving radar platform is utilized to detect localized targets situated in a ROI. We use $p(t)$ and $P(\omega)$ to denote the transmitted time-domain source pulse and its frequency spectrum respectively, where

$$P(\omega) = \int_{\mathbb{R}} p(t) \mathrm{e}^{-\mathrm{j}\omega t} \, \mathrm{d}t. \tag{1}$$

For a localized target whose phase center is situated at $\boldsymbol{l}$, the scattered field at $\boldsymbol{r}'$ due to the excitation pulse emitted at $\boldsymbol{r}$ can be estimated using the first order Born approximation as [11]

$$Y_{\boldsymbol{l}}(\omega, \boldsymbol{r}, \boldsymbol{r}') = P(\omega) S(\omega, \boldsymbol{l}) G(\omega, \boldsymbol{l}, \boldsymbol{r}) G(\omega, \boldsymbol{r}', \boldsymbol{l}) + o, \tag{2}$$

where $S(\omega, \boldsymbol{l})$ is a complex-valued function of frequency and it accounts for all terms introduced by the asymptotic approximation; $G(\omega, \boldsymbol{l}, \boldsymbol{r})$ accounts for propagation from the transmitter at $\boldsymbol{r}$ to the target at $\boldsymbol{l}$; $G(\omega, \boldsymbol{r}', \boldsymbol{l})$ accounts for propagation from the target at $\boldsymbol{l}$ to the receiver at $\boldsymbol{r}'$; and o is the received noise. Further more, for the mono-static radar we assume $\boldsymbol{r}' = \boldsymbol{r}$. Consequently, $G(\omega, \boldsymbol{l}, \boldsymbol{r})$ and $G(\omega, \boldsymbol{r}', \boldsymbol{l})$ can be unified and represented by

$$G(\omega, \boldsymbol{l}, \boldsymbol{r}) = G(\omega, \boldsymbol{r}', \boldsymbol{l}) = a(\boldsymbol{r}, \boldsymbol{l}) \mathrm{e}^{-j\omega \|\boldsymbol{r}-\boldsymbol{l}\|/c}, \tag{3}$$

where $a(\boldsymbol{r}, \boldsymbol{l})$ accounts for the over all magnitude attenuation caused by the antenna beampattern and the propagation between $\boldsymbol{r}$ and $\boldsymbol{l}$, and $\mathrm{e}^{-j\omega\|\boldsymbol{r}-\boldsymbol{l}\|/c}$ is the phase change term of the received signal relative to the source pulse after propagating distance $\|\boldsymbol{r} - \boldsymbol{l}\|$ at speed c.

Without loss of generality we assume there are up to K localized targets, each with a phase center located at a pixel in the ROI image. Let $i_k \in \{1, ..., I\}$ be the pixel index of the kth target and $\boldsymbol{l}_{i_k}$ be the corresponding location. Ideally the mono-static radar performs as a uniform linear array, with the nth antenna located at $\boldsymbol{r}_n$, for $n = 1, 2, ...N$. Due to position perturbations, the actual measurements are taken at $\widetilde{\boldsymbol{r}}_n = \boldsymbol{r}_n + \boldsymbol{\varepsilon}_n$, where $\boldsymbol{\varepsilon}_n$ stands for the unknown position perturbation of the nth antenna with $0 \leq |\boldsymbol{\varepsilon}_n| \leq 10\lambda$, and λ is the wavelength of the radar central frequency. The overall signal received by the perturbed array is then a superposition of scattered waves from all targets in the ROI. We consider measurements at discrete frequency ω_m, where $m = 1, 2, ..., M$. After range compression, we achieve an $M \times N$ data matrix $\widetilde{\mathbf{Y}}$ whose entry (m, n) is

$$\widetilde{Y}_{m,n} = \sum_{k=1}^{K} |P(\omega_m)|^2 S(\omega_m, \boldsymbol{l}_{i_k}) a^2(\widetilde{\boldsymbol{r}}_n, \boldsymbol{l}_{i_k}) \mathrm{e}^{-\mathrm{j}\omega_m \frac{2\left\|\widetilde{\boldsymbol{r}}_n - \boldsymbol{l}_{i_k}\right\|}{c}}. \tag{4}$$

To simplify the expression of acquired data, we define an $M \times 1$ unit vector

$$\phi_{i_k} = \begin{bmatrix} \frac{|P(\omega_1)|^2 S(\omega_1, \boldsymbol{l}_{i_k})}{\sum_{m=1}^{M} |P^2(\omega_m) S(\omega_m, \boldsymbol{l}_{i_k})|^2} \\ \frac{|P(\omega_2)|^2 S(\omega_2, \boldsymbol{l}_{i_k})}{\sum_{m=1}^{M} |P^2(\omega_m) S(\omega_m, \boldsymbol{l}_{i_k})|^2} \\ \vdots \\ \frac{|P(\omega_M)|^2 S(\omega_M, \boldsymbol{l}_{i_k})}{\sum_{m=1}^{M} |P^2(\omega_m) S(\omega_m, \boldsymbol{l}_{i_k})|^2} \end{bmatrix}, \tag{5}$$

an $M \times 1$ exponential vector

$$\widetilde{\psi}_{i_k}^{(n)} = \begin{bmatrix} \mathrm{e}^{-\mathrm{j}\omega_1 \frac{2\left\|\widetilde{\boldsymbol{r}}_n - \boldsymbol{l}_{i_k}\right\|}{c}} \\ \mathrm{e}^{-\mathrm{j}\omega_2 \frac{2\left\|\widetilde{\boldsymbol{r}}_n - \boldsymbol{l}_{i_k}\right\|}{c}} \\ \vdots \\ \mathrm{e}^{-\mathrm{j}\omega_M \frac{2\left\|\widetilde{\boldsymbol{r}}_n - \boldsymbol{l}_{i_k}\right\|}{c}} \end{bmatrix}, \tag{6}$$

and a scaler

$$x_{i_k}^{(n)} = a^2(\widetilde{\boldsymbol{r}}_n, \boldsymbol{l}_{i_k}) \sum_{m=1}^{M} |P^2(\omega_m) S(\omega_m, \boldsymbol{l}_{i_k})|^2. \tag{7}$$

The nth column of $\widetilde{\mathbf{Y}}$ can then be written in a matrix-vector form as

$$\widetilde{\mathbf{y}}^{(n)} = \sum_{k=1}^{K} (\phi_{i_k} \circ \widetilde{\psi}_{i_k}^{(n)}) \cdot x_{i_k}^{(n)} = (\boldsymbol{\Phi} \circ \widetilde{\boldsymbol{\Psi}}^{(n)}) \mathbf{x}^{(n)} = \widetilde{\boldsymbol{\Gamma}}^{(n)} \mathbf{x}^{(n)}, \tag{8}$$

where the symbol $\circ$ represents element-wised product. Here $\widetilde{\boldsymbol{\Gamma}}^{(n)} = [\phi_{i_1} \circ \widetilde{\psi}_{i_1}^{(n)}, ..., \phi_{i_K} \circ \widetilde{\psi}_{i_K}^{(n)}]$ is an $M \times K$ projection matrix of the nth antenna position, $\mathbf{x}^{(n)} = [x_{i_1}^{(n)}, ..., x_{i_K}^{(n)}]^T$ is a $K \times 1$ vector of target scattering coefficients. It is important to note that ϕ_{i_k} is a target signature vector independent of antenna positions.

III. Sparsity driven Auto-focus imaging

A. Optimization problem

Since the antenna positions $\widetilde{\boldsymbol{r}}_n$ are not known exactly, imaging formation that treats the perturbed array as a uniform array generally yields a de-focused image with its image quality related to the position perturbations. In order to perform imaging with autofocus, we solve the following sparsity constrained optimization problem

$$\min_{\widetilde{\boldsymbol{\Gamma}}^{(n)}, \mathbf{x}^{(n)}} \sum_{n=1}^{N} \|\widetilde{\mathbf{y}}^{(n)} - \widetilde{\boldsymbol{\Gamma}}^{(n)} \mathbf{x}^{(n)}\|_2^2, \quad \text{s.t.} \quad \|\sum_{n=1}^{N} \mathbf{x}^{(n)}\|_0 < K. \tag{9}$$

The above optimization problem is similar to the group sparsity formulation that is often used in CS imaging [12] in the aspect that all unknown vectors share the same non-zero support but have generally different values within the support. However, the auto-focus problem we are trying to solve here is more general than the group sparsity problem since the projection matrices are not identical across all antennas. They share the same target signature vector ϕ_{i_k}, but are different in the unknown exponential term $\widetilde{\psi}_{i_k}$. To solve (9), we re-organize the data matrix $\widetilde{\mathbf{Y}}$ as

$$\widetilde{\mathbf{Y}} = \sum_{k=1}^{K} [x_{i_k}^{(1)} \phi_{i_k}, ..., x_{i_k}^{(N)} \phi_{i_k}] \circ [\widetilde{\psi}_{i_k}^{(1)}, ..., \widetilde{\psi}_{i_k}^{(N)}] = \sum_{k=1}^{K} \mathbf{E}_{i_k} \circ \widetilde{\boldsymbol{\Psi}}_{i_k}, \tag{10}$$

where $\mathbf{E}_{i_k} = [x_{i_k}^{(1)} \cdot \phi_{i_k}, ..., x_{i_k}^{(N)} \cdot \phi_{i_k}]$ is an $M \times N$ rank-one matrix whose dominant left singular vector is exactly ϕ_{i_k}, and $\widetilde{\boldsymbol{\Psi}}_{i_k} = [\widetilde{\psi}_{i_k}^{(1)}, ..., \widetilde{\psi}_{i_k}^{(N)}]$ is an $M \times N$ exponential matrix parameterized by the distance between the kth target and the perturbed antennas. Equation (9) can be equivalently written as

$$\min_{\mathbf{E}_{i_k}, \widetilde{\boldsymbol{\Psi}}_{i_k}} \|\widetilde{\mathbf{Y}} - \sum_{k=1}^{K} \mathbf{E}_{i_k} \circ \widetilde{\boldsymbol{\Psi}}_{i_k}\|_F^2, \quad \text{s.t.} \quad \text{rank}(\mathbf{E}_{i_k}) = 1, \tag{11}$$

where the subscript F represents the Frobenius norm.

Motivated by the orthogonal matching pursuit algorithm, we solve the above optimization problem iteratively. In particular, we first analyze the coherence of measured data to have a warm start in estimating the first target phase center. Then we repeat the following steps iteratively, for $k = 1, 2..., K$, until convergence:

1) Locate $\boldsymbol{l}_{i_k}$ on the current residual image,
2) Estimate $\widetilde{\boldsymbol{\Psi}}_{i_k}$ with data coherence analysis,
3) Estimate $\mathbf{E}_{i_k}$ and extract target signature ϕ_{i_k},
4) Update $\widetilde{\boldsymbol{r}}_k^{(n)}$ and $\boldsymbol{l}_{i_k}$,
5) Reconstruct a sparse image and a dense radar image,
6) Update residuals for the next iteration.

The details of these steps are explained in the following sub-sections.

B. Data coherence anaysis

Assume that at the kth iteration, we reconstruct an image $\widehat{\mathbf{x}}_{\text{res},k}$ using the residual data $\mathbf{y}_{\text{res},k-1}^{(n)}$, which is initialized as measured data. A new target is then detected at location $\boldsymbol{l}_{i_k}$ where

$$i_k = \underset{i}{\text{argmax}} \{|\widehat{\mathbf{x}}_{\text{res},k}(i)|\}. \tag{12}$$

It is well known that cross-correlation(CC) is a measure of similarity of two series as a function of the lag of one relative to the other. The maximum of the CC function indicates the point in time where the signals are best aligned. In the radar imaging process, the phase

changes, or the lags of scattered waves from a target measured by perturbed antennas are determined by the distances between the target and the perturbed antennas. Therefore, the perturbations can be estimated by analyzing the coherence of the corresponding scattered signals via the CC function. To reduce the ambiguity of the CC function, we extract the kth target response using time gating

$$\widehat{y}_{i_k}^{(n)}(t) = \begin{cases} y_{\text{res},k-1}^{(n)}(t), & |t-\tau_{i_k}^{(n)}| \le \frac{20\lambda}{c} \\ 0, & |t-\tau_{i_k}^{(n)}| > \frac{20\lambda}{c} \end{cases}, \tag{13}$$

where $y_{\text{res},k-1}^{(n)}(t)$ is the time-domain residual signal, and $\tau_{i_k}^{(n)} = \frac{2\|\boldsymbol{r}_n - \boldsymbol{l}_{i_k}\|}{c}$. Note that the time-gating boundary $\frac{20\lambda}{c}$ is determined by the maximum position perturbation, and it can be tightened by considering the smooth trajectory of the radar platform. We then take $\widehat{y}_{i_k}^{([\frac{N}{2}])}(t)$ as a reference, where $[\frac{N}{2}]$ is the largest integer not greater than $\frac{N}{2}$, and estimate the time shift of $\widehat{y}_{i_k}^{(n)}(t)$ in (13) as

$$\widehat{\tau}_{n,[\frac{N}{2}]} = \underset{\tau}{\text{argmax}} \int \widehat{y}_{i_k}^{(n)}(t) \cdot \widehat{y}_{i_k}^{([\frac{N}{2}])}(t+\tau)dt. \tag{14}$$

Let $\widetilde{\tau}_{i_k}^{(n)} = \frac{2\|\widetilde{\boldsymbol{r}}_n - \boldsymbol{l}_{i_k}\|}{c}$ represent the unknown pulse propagation time from $\widetilde{\boldsymbol{r}}_n$ to $\boldsymbol{l}_{i_k}$ and back to $\widetilde{\boldsymbol{r}}_n$. Based on (14), and assuming the total propagation time is the same as that of the ideal uniform array, we have the following equations to solve $\widetilde{\tau}_{i_k}^{(n)}$ for $n = 1, 2, ..., N$, such that the signals in (13) are coherent at $\boldsymbol{l}_{i_k}$ after back-propagation,

$$\begin{cases} \widetilde{\tau}_{i_k}^{(n)} - \widetilde{\tau}_{i_k}^{[N/2]} = \widehat{\tau}_{n,[\frac{N}{2}]}, \text{ for } n \neq [\frac{N}{2}] \\ \sum_{n=1}^{N} \widetilde{\tau}_{i_k}^{(n)} = \sum_{n=1}^{N} \tau_{i_k}^{(n)} \end{cases}. \tag{15}$$

With the solution of (15), $\widetilde{\psi}_{i_k}^{(n)}$ is computed using (6).

C. Target signature extraction

Given $\widetilde{\boldsymbol{\Psi}}_{i_k}$, we determine $\mathbf{E}_{i_k}$ by minimizing the following degenerated objective function of (11)

$$\mathbf{E}_{i_k} = \underset{\mathbf{E}}{\text{argmin}} \|\widetilde{\mathbf{Y}}_{\text{res},k} - \mathbf{E} \circ \widetilde{\boldsymbol{\Psi}}_{i_k}\|_F^2 \text{ s.t. } \text{rank}(\mathbf{E}) = 1. \tag{16}$$

This optimization problem can be solved by using the singular value decomposition (SVD) of $\overline{\mathbf{Y}}_{\text{res},k} = \widetilde{\mathbf{Y}}_{\text{res},k} \circ \widetilde{\boldsymbol{\Psi}}_{i_k}^*$ [13]:

$$\overline{\mathbf{Y}}_{\text{res},k} = \mathbf{U}_k \boldsymbol{\Sigma}_k \mathbf{V}_k^H, \tag{17}$$

where the superscripts $*$ and H represent the phase conjugate and the Hermitian transpose respectively. Based on the SVD, we have

$$\mathbf{E}_{i_k} = \sigma_{k1} \mathbf{u}_{k1} {\mathbf{v}_{k1}}^H, \tag{18}$$

where σ_{k1} is the largest singular value of $\overline{\mathbf{Y}}_{\text{res},k}$ representing the scattering strength of the kth target, $\mathbf{u}_{k1}$ is the corresponding left singular vector representing the target signature, *i.e.*

$$\widehat{\phi}_{i_k} = \mathbf{u}_{k1}, \tag{19}$$

and $\mathbf{v}_{1,i_k}^H$ is the corresponding right singular vector related to the antenna pattern.

D. Antenna position estimation

Based on the propagation time between each antenna and the k detected targets, we estimate the antenna positions as

$$\begin{aligned} \widehat{\boldsymbol{r}}_k^{(n)} =& \underset{\boldsymbol{r}}{\text{argmin}} |\langle \boldsymbol{r} - \boldsymbol{r}_n, \frac{\boldsymbol{r}_{n+1} - \boldsymbol{r}_n}{\|\boldsymbol{r}_{n+1} - \boldsymbol{r}_n\|} \rangle|^2 \\ &+ \sum_{k'=1}^{k} \frac{\sigma_{k'1}}{\sum_{k'=1}^{k} \sigma_{k'1}} \left(\|\boldsymbol{r} - \boldsymbol{l}_{i_{k'}}\| - \frac{\widetilde{\tau}_{i_{k'}}^{(n)} c}{2} \right)^2. \end{aligned} \tag{20}$$

The above cost function is composed of two parts. The first part minimizes the azimuth discrepancy between the nth perturbed antenna position and its ideal position. The second part restricts the distance in the range direction according to the propagation time. We use normalized target strength $\sigma_{k'1}/(\sum_{k'=1}^{k} \sigma_{k'1})$ to weight the second part considering that stronger scattering targets are more likely well located and less likely to be interfered by noise than weaker targets in our iterative approach. While the cost function in (20) is not convex, a global optimal solution may be achievable using the algorithm in [14] with a proper initial value of $\boldsymbol{r}$. Note that since the antenna locations are determined based on distance measurements, which are translation and rotation invariant, we assume in our simulations the mean and the dominant orientation of the perturbed array are the same as the ideal uniform array. The translation and the rotation effects of the perturbed antennas can be removed while keeping the distances between the perturbed antennas and the targets unchanged by a liner transform on the antenna and target locations simultaneously.

E. Image reconstruction

Given the estimated projection matrix

$$\widehat{\boldsymbol{\Gamma}}_k^{(n)} = \left[\widehat{\phi}_{i_1} \circ \widetilde{\psi}_{i_1}^{(n)}, \widehat{\phi}_{i_2} \circ \widetilde{\psi}_{i_2}^{(n)}, ..., \widehat{\phi}_{i_k} \circ \widetilde{\psi}_{i_k}^{(n)} \right], \tag{21}$$

scattering coefficients are computed using least squares

$$\widehat{\mathbf{x}}_k^{(n)} = (\widehat{\boldsymbol{\Gamma}}_k^{(n)})^\dagger \widetilde{\mathbf{y}}^{(n)}, \tag{22}$$

where $\widehat{\mathbf{x}}_k^{(n)}$ is a $k \times 1$ vector representing the scattering coefficients of the k detected targets and the superscript $\dagger$ denotes the Penrose-Moore inverse. A sparse image $\widehat{\mathbf{x}}_{\text{s},k}$ of the ROI is then reconstructed by assigning $\widehat{\mathbf{x}}_k^{(n)}$ to the corresponding pixel locations, *i.e.*

$$\widehat{\mathbf{x}}_{\text{s},k}(i_{k'}) = \sum_{n=1}^{N} \widehat{\mathbf{x}}_k^{(n)}(k'), \text{for } k' = 1, ..., k. \tag{23}$$

For the purpose of target recognition, a dense image preserving target signature information can also be reconstructed by incorporating target signatures. We first reconstruct data of the ideal uniform array using the signatures of the k detected targets as follows

$$\widehat{\mathbf{y}}_k^{(n)} = \sum_{k'=1}^{k} \widehat{x}_{i_{k'}}^{(n)} \cdot (\widehat{\phi}_{i_{k'}} \circ \psi_{i_{k'}}^{(n)}), \tag{24}$$

where $\psi_{i_{k'}}^{(n)}$ has the same expression as $\widetilde{\psi}_{i_k}^{(n)}$ except using the uniform antenna position $\boldsymbol{r}_n$. Based on the reconstructed data, we then perform delay-and-sum imaging to reconstruct a dense image

$$\widehat{\mathbf{x}}_{\text{d},k} = \sum_{n=1}^{N} \left(\boldsymbol{\Psi}^{(n)} \right)^H \widehat{\mathbf{y}}_k^{(n)}, \tag{25}$$

where $\boldsymbol{\Psi}^{(n)}$ is an $M \times I$ exponential matrix related to the ideal uniform array and the whole ROI.

F. Initialization, iteration, and termination

Since the position perturbations can be several-wavelength large, radar targets may be not resolvable on the initial image without any phase compensation. In order to have a warm start for our iterative algorithm, we first perform coherence analysis on measured data such that their overall lags can be approximately compensated.

To iteratively exploit targets, we compute the residual signal of the nth antenna for the next iteration by removing the signals of all the detected targets

$$\mathbf{y}_{\text{res},k}^{(n)} = \mathbf{y}^{(n)} - \widehat{\boldsymbol{\Gamma}}_k^{(n)} \widehat{\mathbf{x}}_k^{(n)}. \tag{26}$$

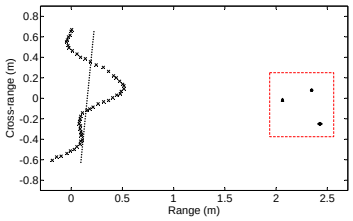

Fig. 1. Setup of mono-static radar imaging.

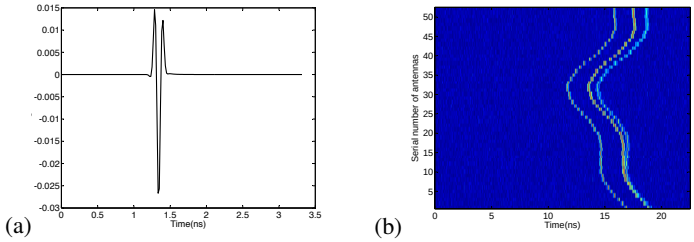

Fig. 2. (a) Emitted pulse and (b) Simulated noisy radar echoes.

The residual image is then updated as

$$\widehat{\mathbf{x}}_{\text{res},k+1} = \sum_{n=1}^{N} (\widehat{\mathbf{\Psi}}_k^{(n)})^H \mathbf{y}_{\text{res},k}^{(n)}, \tag{27}$$

The algorithm is terminated when the preset sparsity level is met or no more targets are identified, *i.e.*, mathematically when $k = K$ or $\frac{\sigma_{k1}-\sigma_{k2}}{\sigma_{k1}} < \epsilon$ is satisfied. Here σ_{k2} is the second largest singular value of $\overline{\mathbf{Y}}_{\text{res},k}$, and ϵ is a threshold with value $0 < \epsilon < 1$.

IV. Numerical Simulations

The simulation setup is depicted in Fig. 1, where we use black dots to indicate ideal antenna positions, and x-marks to indicate perturbed antenna positions. We note that the antenna perturbations are up to 10λ. A differential Gaussian pulse, illustrated in Fig. 2(a), is emitted to illuminate the ROI. The received signals are simulated using the free-space Green's function with added white Gaussian noise. Fig. 2(b) shows the simulated signal with PSNR=25dB.

In our auto-focus approach, we set the total number of targets $K = 50$ and the stop threshold $\epsilon = 0.2$. The imaging results are plotted in Fig. 3 with 30 dB dynamic range. In particular, Fig. 3(a) shows the imaging result using the conventional delay-and-sum method, ignoring unknown positions errors. Figure 3(b) shows the imaging result with initial phase-compensation using coherence analysis for a focus point at the center of the ROI. We can see that the image focus is better overall, but the three off-center targets are still not well focused. In stead, when we use our proposed approach, the sparse image is reconstructed using (23) as shown in Fig. 3(c), where each circle represents a sparse target, with the circle center corresponding to the target phase center and the circle size proportional to the target scattering coefficient. The dense image with target signatures using (25) is reconstructed as shown in Fig. 3(d). For comparison, we plot the result using the conventional delay-and-sum imaging method given the exactly perturbed position errors in Fig. 3(e); and the benchmark result of the ideal uniform array in Fig. 3(f). We can notice that our imaging result in Fig. 3(d) with target signatures is visually very close to that of the ideal uniform array shown in Fig. 3(f), and even better than the result of known position errors shown in Fig. 3(e) in reducing target sidelobes. This is because

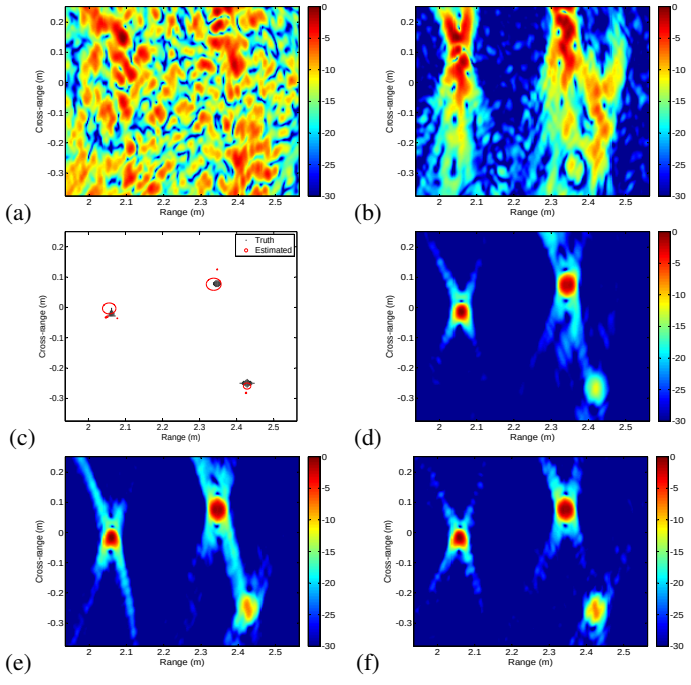

Fig. 3. Imaging results: (a) delay-and-sum imaging with uniform array Green's function; (b) imaging with initial phase compensation; (c) CS with image-domain sparsity; (d) dense image with target signatures; (e) imaging with known position errors; (f) imaging with ideal uniform array data

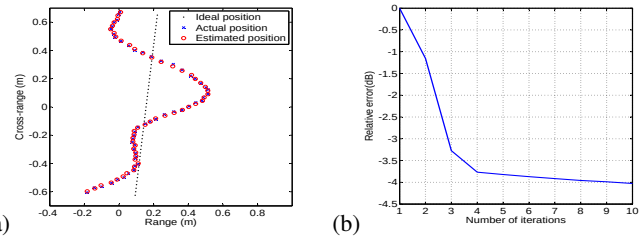

Fig. 4. (a) Comparison of ideal, actual, and estimated antenna positions, and (b) Relative reconstruction error of iterative autofocus algorithm

our image is based on reconstructed data of the ideal uniform array, which typically exhibits smaller sidelobes than a random array of the same aperture size [15]. The performance of our method is also verified by position estimation and relative error reduction. In Fig. 4 (a) we observed good agreement between the estimated and the actual antenna positions. Figure 4 (b) shows the relative error of the residual data relative to the original measured data. The curve shows that our method converges in only several iterations.

V. Conclusions

We propose a sparsity-driven radar auto-focus imaging approach for unknown position errors up to several wavelengths. Our auto-focus approach is realized by building an adaptive projection matrix of target signatures via data coherence analysis, and imposing sparsity on the reflectivity to be reconstructed. Both the sparse image of target phase centers and the dense image with target signatures can be reconstructed efficiently using our proposed approach. Imaging results using simulated noisy data of a mono-static radar demonstrate auto-focus ability and computational efficiency of our approach in imaging localized targets even under up to 10 wavelength position perturbations.

REFERENCES

[1] D. E. Wahl, P. H. Eichel, D. C. Ghiglia, and C. V. Jakowatz Jr, "Phase gradient autofocus - a robust tool for high resolution SAR phase correction," *IEEE Trans. Aerospace and Electronic Systems*, vol. 30, no. 3, pp. 827–835, 1994.

[2] X. Li, G. Liu, and J. Ni, "Autofocusing of ISAR images based on entropy minimization," *IEEE Trans. Aerospace and Electronic Systems*, vol. 35(4), pp. 1240–1252, October 1999.

[3] W. Ye, T.S. Yeo, and Z. Bao, "Weighted least-squares estimation of phase errors for SAR/ISAR autofocus," *IEEE Trans. Geoscience and Remote Sensing*, vol. 37(5), pp. 2487–2494, September 1999.

[4] F. Berizzi, M. Martorella, A. Cacciamano, and A. Capria, "A contrast-based algorithm for synthetic range-profile motion compensation," *IEEE Trans. Geoscience and Remote Sensing*, vol. 46(10), pp. 3053–3062, October 2008.

[5] M. P. Nguyen and S. B. Ammar, "Second order motion compensation for squinted spotlight synthetic aperture radar," in *Asia-Pacific Conference on Synthetic Aperture Radar(APSAR)*, Sept 2013.

[6] J. Yang, X. Huang, J. Thompson, T. Jin, and Z Zhou, "Compressed sensing radar imaging with compensation of observation position error," *IEEE Trans. Geoscience and Remote Sensing*, vol. 52(8), pp. 4608–4620, August 2014.

[7] X. Du, C. Duan, and W. Hu, "Sparsity representation based autofocusing technique for ISAR images," *IEEE Trans. Geoscience and Remote Sensing*, vol. 51(3), pp. 1826–1835, March 2013.

[8] N. O. Onhon and M. Cetin, "A sparsity-driven approach for joint SAR imaging and phase error correction," *IEEE Trans. Image Processing*, vol. 21(4), pp. 2075–2088, April 2012.

[9] Y. Chi, L. L. Scharf, A. Pezeshki, and A. R. Calderbank, "Sensitivity to basis mismatch in compressed sensing," *IEEE Trans. Signal Processing*, vol. 59(5), pp. 2182–2195, May 2011.

[10] Y. Tang, L. Chen, and Y. Gu, "On the performance bound of sparse estimation with sensing matrix perturbation," *IEEE Trans. Signal Processing*, vol. 61(17), pp. 4372–4386, September 2013.

[11] D. Liu, G. Kang, L. Li, Y. Chen, S. Vasudevan, W. Joines, Q. Liu, J. Krolik, and L. Carin, "Electromagnetic time-reversal imaging of a target in a cluttered environment," *IEEE Trans. Antennas Propagat.*, vol. 53, pp. 3058–3066, Sept. 2005.

[12] L. Meier S. van de Geer and P. Bühlmann, "The group lasso for logistic regression," *Journal of the Royal Statistical Society: Series B (Statistical Methodology)*, vol. 70, pp. 53–71, February 2008.

[13] P. de Groen, "An introduction to total least squares," *Nieuw Archief voor Wiskunde*, vol. 14, pp. 237–253, July 1996.

[14] A. Beck, P. Stoica, and J. Li, "Exact and approximate solutions of source localization problems," *IEEE trans. Signal Processing*, vol. 56(5), pp. 1770–1777, May 2008.

[15] B. D. Steinberg, "The peak sidelobe of the phased array having randomly located elements," *IEEE Trans. Antennas and Propagation*, vol. 20(2), pp. 129–136, March 1972.